Establishment of radioactive astatine and iodine uptake in cancer cell lines expressing the human sodium/iodide symporter

T. Petrich, H.-J. Helmeke, G. J. Meyer, W. H. Knapp, E. Pötter

Department of Nuclear Medicine, Medizinische Hochschule Hannover, Carl-Neuberg-Strasse 1, 30625 Hannover, Germany

Received 20 October 2001 and in revised form 28 January 2002 / Published online: 11 April 2002

Abstract. The sodium/iodide symporter (NIS) has been recognized as an attractive target for radioiodine-mediated cancer gene therapy. In this study we investigated the role of human NIS for cellular uptake of the high LET α-emitter astatine-211 (^{211}At) in comparison with radioiodine as a potential radionuclide for future applications. A mammalian NIS expression vector was constructed and used to generate six stable NIS-expressing cancer cell lines (three derived from thyroid carcinoma, two from colon carcinoma, one from glioblastoma). Compared with the respective control cell lines, steady state radionuclide uptake of NIS-expressing cell lines increased up to 350-fold for iodine-123 (^{123}I), 340-fold for technetium-99m pertechnetate ($^{99m}TcO_4^-$) and 60-fold for ^{211}At. Cellular ^{211}At accumulation was found to be dependent on extracellular Na^+ ions and displayed a similar sensitivity towards sodium perchlorate inhibition as radioiodide and $^{99m}TcO_4^-$ uptake. Heterologous competition with unlabelled NaI decreased NIS-mediated ^{211}At uptake to levels of NIS-negative control cells. Following uptake both radioiodide and ^{211}At were rapidly (apparent $t_{1/2}$ 3–15 min) released by the cells as determined by wash-out experiments. Data of scintigraphic tumour imaging in a xenograft nude mice model of transplanted NIS-modified thyroid cells indicated that radionuclide uptake in NIS-expressing tumours was up to 70 times (^{123}I), 25 times ($^{99m}TcO_4^-$) and 10 times (^{211}At) higher than in control tumours or normal tissues except stomach (3–5 times) and thyroid gland (5–10 times). Thirty-four percent and 14% of the administered activity of ^{123}I and ^{211}At, respectively, was found in NIS tumours by region of interest analysis (n=2). Compared with cell culture experiments, the effective half-life in vivo was greatly prolonged (6.5 h for ^{123}I, 5.2 h for ^{211}At) and preliminary dosimetric calculations indicate high tumour absorbed doses (3.5 Gy/MBq$_{tumour}$ for ^{131}I and 50.3 Gy/MBq$_{tumour}$ for ^{211}At). In conclusion, NIS-expressing tumour cell lines of different origin displayed specific radionuclide uptake in vitro and in vivo. We provide first direct evidence that the high-energy α-emitter ^{211}At is efficiently transported by NIS. Application of ^{211}At may direct higher radiation doses to experimental tumours than those calculated for ^{131}I. Thus, ^{211}At may represent a promising alternative radionuclide for future NIS-based tumour therapy.

Keywords: Sodium/iodide symporter – Gene therapy – Radioiodine – Astatine – Cancer

Eur J Nucl Med (2002) 29:842–854
DOI 10.1007/s00259-002-0784-7

E. Pötter (✉)
Department of Nuclear Medicine,
Medizinische Hochschule Hannover, Carl-Neuberg-Strasse 1,
30625 Hannover, Germany
e-mail: potter.eyck@mh-hannover.de
Tel.: +049-511-5322675, Fax: +049-511-5322591

Introduction

Active transport and organification of iodide in the thyroid form the physiological basis for radioiodine therapy of differentiated thyroid carcinomas and their metastases [1]. Driven by the energy of the transmembrane Na^+ gradient, iodide is actively transported across the basolateral plasmamembrane of thyrocytes together with Na^+ ions by the sodium/iodide symporter (NIS), which has been cloned recently in rat, man and mouse [2, 3, 4, 5]. Mediated by an apical anion transporter, iodide enters the lumen of the thyroid follicle, where it is organified in the course of thyroid hormone biosynthesis by subsequent oxidation and transfer onto tyrosyl residues of thyroglobulin (TG) catalysed by thyroid peroxidase (TPO) (for reviews see [6, 7]). Besides the thyroid as the main organ in which NIS is expressed at high levels, several other tissues have been found to contain NIS mRNA or protein as well, including salivary gland, gastric mucosa, lactating breast and kidney [8, 9, 10, 11]. In principle, such

tissues may be negatively affected by high-dose radioiodine therapy, but the differential radioiodine uptake of most thyroid carcinomas and normal non-thyroid tissue is in general sufficient to treat even extensive disease with tolerable side-effects [1, 12].

As down-regulated or mis-targeted NIS expression is commonly found in thyroid carcinomas and frequently correlates with tumour dedifferentiation and with loss of radioiodine uptake capacity, NIS represents a key protein for thyroid cancer therapy and diagnosis [3, 13, 14, 15, 16, 17, 18]. Even though most underlying mechanisms are largely unknown, studies so far indicate that decreased NIS gene expression in thyroid cancer progression is not related to irreversible mutational inactivation but to dysregulation or epigenetic mechanisms, including aberrant NIS promoter hypermethylation, which might form the basis for redifferentiation therapy strategies [19, 20, 21, 22, 23, 24].

Since the radioiodine therapy regimen is well defined and widely established, it has been recognized that the NIS gene is an attractive target for general radioiodine-mediated cancer gene therapy. One basic requirement for this hypothetical transfer of radioiodine therapy with simple molecules (i.e. $Na^{131}I$) to non-thyroid tumours is that tumour cells must be genetically modified to express NIS, as has already been demonstrated in a variety of recent studies by viral or non-viral transfer of NIS expression vectors [25, 26, 27, 28, 29, 30, 31, 32, 33, 34, 35, 36]. Apart from problems concerning complete vector delivery and specific tumour targeting, radioiodine tumour therapy might be hampered by the short effective half-life of radioiodine in non-thyroid or dedifferentiated thyroid tumour cells due to failing organification. Accordingly, most studies report rapid radioiodine loss from transfected cells and intratumoural residence times insufficient to deliver tumouricidal doses in vivo [26, 27, 28, 29, 30, 32, 35]. Therefore, the application of high-energy α-emitters with a short physical half-life, such as the cyclotron product astatine-211 (^{211}At) might be more appropriate than iodine-131 (^{131}I) provided that modified tumour cells are capable of transporting radioastatine. Although it is well known from cell culture and animal experiments that ^{211}At, most likely in the form of astatide, accumulates in the thyroid like iodide and pertechnetate [37, 38, 39, 40], no direct evidence currently exists that ^{211}At is transported by NIS. In this study we investigated the uptake characteristics of radioastatine in comparison with radioiodine as well as pertechnetate in vitro and in vivo using NIS-expressing cell lines representing different forms of cancer; in particular we aimed to determine the role of NIS in intracellular accumulation and the differential radiation doses to experimental tumours with these agents.

Materials and methods

Construction of an NIS expression vector. Human thyroid total RNA was reverse transcribed into cDNA using oligo(dT) primers and Superscript RT II according to the manufacturer's protocol (Gibco Life Technologies). Two overlapping 1-kb cDNA fragments representing either the 5′-half or the 3′-half of the complete human NIS coding region were amplified from the cDNA template by PCR using Pfu DNA-Polymerase (Stratagene, Amsterdam, The Netherlands) with respective primer combinations 347F/1367R and 1342F/2370R (primer sequences: 347F: 5′-CATGGACGCCGTGGAGACCGG-3′; 1367R: 5′-GGGGACTCCAGGCAGATCTTCG-3′; 1342F: 5′-TCTTCGAAGATCTGCCTGGAGTCC-3′; 2370R: 5′-AATCAGAGCCCAAGGCCATGG-3′) and PCR conditions as follows: 4 min 94°C pre-denaturation; 35 cycles each of 1 min 94°C denaturation, 20 s 62°C annealing, 2.5 min 72°C extension; 10 min 72°C final extension. Both amplified fragments were subcloned in the vector pCR-Blunt (Invitrogen, Leek, The Netherlands). The nucleotide sequences of recombinant plasmids were determined using the Thermo sequenase radiolabelled terminator cycle sequencing kit (Amersham Life Sciences, Freiburg, Germany). An NIS full-length clone was constructed by in-frame fusion of both halves using a unique *Bgl*II site in the overlap of the fragments and subsequently the complete coding region was subcloned in both orientations into the *Eco*RI site of the pCIneo expression vector (Promega, Mannheim, Germany). Plasmid DNA used for transfections was purified using a commercial kit (Endo-free kit, Qiagen, Hilgen, Germany).

Cell culture and generation of human NIS-expressing cell lines. Human cell lines were obtained from ECACC (Salesbury, UK) and DSMZ (Braunschweig, Germany) and included the papillary thyroid carcinoma cell lines B-CPAP (DSMZ no. ACC273) and K1 (ECACC no. 92030501), the undifferentiated thyroid carcinoma cell line 8505-C (DSMZ no. ACC219), the colon adenocarcinoma cell lines SW480 (DSMZ no. ACC313) and CACO-2 (DSMZ no. ACC169) and the glioblastoma cell line DBTRG-05MG (DSMZ no. ACC359). Cell lines were maintained in tissue culture plates at 37°C in a humidified atmosphere with 5% CO_2 using recommended growth media [RPMI1640 for B-CPAP, 8505-C, SW480, DBTRG-05MG; DMEM/HamF12/MCDB104 (2:1:1) plus 2 m*M* glutamine for K1; MEM for CACO-2] and supplementation (10% FBS, 100 IU/ml penicillin; 100 µg/ml streptomycin). Cells (1×10^6) were plated in 10-cm plates 1 day before transfection. Three micrograms of purified pCIneo vector DNA or pCIneo-NIS DNA was transfected using Fugene 6 (Roche Diagnostics, Mannheim, Germany) according to the manufacturer's protocol. Forty-eight hours post transfection, antibiotic selection was started by addition of 500 µg/ml Geneticin (G418, Calbiochem). Surviving colonies were isolated by cloning cylinders after 4–8 weeks' growth, expanded and screened for $NaClO_4$-sensitive $Na^{125}I$ uptake capacity. Five to 25 NIS cell clones were expanded for each cell line along with three to five pCIneo-cell clones; with some of them a secondary subcloning step was performed by limiting dilution followed by a $Na^{125}I$ uptake screen. Resulting cell lines with maximum $Na^{125}I$ uptake values were named K1-NIS, B-CPAP-NIS, 8505-C-NIS, SW480-NIS, DBTRG-NIS, and CACO-2-NIS, and used in combination with the respective parental (for K1 and 8505-C) or stable pCIneo-transfected (for the rest of the cell lines) control cell line in further experiments.

Analysis of mRNA by RT-PCR. Total RNA was prepared from cell lines using a commercial kit (Qiagen, Hilgen, Germany) and quantitated spectrophotometrically. Using 2 µg RNA cDNA was prepared by reverse transcription as described above. cDNA aliquots equivalent to 100 ng RNA were subjected to PCR using Herculase DNA polymerase (Stratagene, Amsterdam, The Netherlands) and

NIS-specific primers 347F/1367R (see above) or β-actin-specific primers (5′-ACACTGTGCCCATCTACGAGG-3′ and 5′-AGGGGCCGGACTCGTCATACT-3′). For NIS amplification, cycling conditions were 3 min at 95°C for pre-denaturation; 40 cycles of 30 s at 94°C for denaturation, 20 s at 62°C for annealing, 80 s at 72°C for extension followed by 10 min at 72°C for final extension. The same PCR conditions except for 33 cycles and extension of 45 s at 72°C were applied for β-actin. PCR products were resolved on agarose gels, stained with ethidium bromide and visualized by UV illumination. Expected product sizes are 1,021 bp for NIS and 621 bp for β-actin.

Antibody generation and immunostaining. A polyclonal human NIS-specific antibody was raised in rabbits using a NIS carboxy-terminal peptide (amino acid sequence in one-letter code: CVGHDGGRDQQETNL) conjugated to keyhole limpet haemocyanin. Peptide synthesis, coupling, immunization and antibody purification by affinity chromatography on a matrix of the peptide coupled to Sepharose were performed by Biotrend KG (Koeln, Germany). For immunohistochemistry, cells grown in four-well chamber slides were fixed (10 min at room temperature; 4% *p*-formaldehyde/PBS), permeabilized (10 min at room temperature; 0.1% Triton ×100/PBS), blocked (30 min at room temperature; 10% normal goat or donkey serum/PBS) and incubated for 2 h with NIS-specific antibody (1:500 dilution in 1% normal donkey serum/PBS). A Vectastain ABC peroxidase kit (Vector Laboratories, Burlingame, Calif., USA) in combination with suitable biotinylated secondary antibody was employed to detect bound primary antibody using 3-3′-diaminobenzidine (DAB) as chromogen according to the manufacturer's instructions. Following counterstaining of cell nuclei with haematoxylin, slides were mounted and photographed on a Zeiss Axiovert microscope equipped with a Spot RT camera (Diagnostic Instruments, Inc., Sterling Heights, USA). Negative controls included omission of primary antibody and substitution with normal rabbit serum. NIS-transfected cells and control cells were grown on the same chamber slide and were processed in parallel as well. For control purposes a mouse monoclonal NIS antibody, hsNIS-FP5a [41], generously provided by Dr. J.C. Morris (Mayo Clinic, Rochester, Minn., USA), was used at a 1:5,000 dilution in parallel stainings and gave the same results.

Radionuclides and ^{211}At production. ^{123}I and ^{125}I as sodium iodide solutions (no carrier added) were obtained from Amersham (Braunschweig, Germany). Technetium-99m pertechnetate ($^{99m}TcO_4^-$) was eluted from a commercially available generator system (Elumatic III, CIS, Berlin, Germany). For ^{211}At production by the ^{209}Bi(α, 2n)^{211}At reaction, external natural bismuth metal targets were irradiated with 10 μA of 27.5 MeV α-particles (~25 MeV on target due to energy losses in foils and He cooling) for 15 min in the department's cyclotron (MC35, Scanditronix). The low on-target energy prevents formation of ^{210}At and ^{210}Po contaminants. ^{211}At was separated from the bismuth target by dry distillation at 850–930°C for 30–40 min, starting from room temperature, in a customized apparatus and collected in 0.02 *M* Na_2SO_3. The procedure was monitored online using a portable Geiger-Mueller counter. Radiochemical purity and quantitation were determined by gamma-spectroscopy. ^{211}At production details will be described elsewhere. Radioactivity concentrations of ^{211}At stock solutions were 7–15 MBq/ml with distillation yields up to 80% of the initial target activity, and were diluted at least 50-fold with bHBSS (see below) before use.

Radionuclide uptake in vitro. Uptake experiments were performed according to Weiss et al. [42] with minor modifications. In brief, cells (10^5/well) were plated in triplicates in 24-well plates (Falcon) in their respective growth medium and 24 h or 48 h later the cells were pre-incubated at 37°C for 30 min in 1 ml HEPES-buffered Hank's balanced salt solution (bHBSS) (137 m*M* NaCl, 5.4 m*M* KCl, 1.3 m*M* $CaCl_2$, 0.4 m*M* $MgSO_4$, 0.5 m*M* $MgCl_2$, 0.4 m*M* Na_2HPO_4, 0.44 m*M* KH_2PO_4, 5.55 m*M* glucose, 10 m*M* HEPES, pH7.3). Cells were incubated at 37°C with 1 ml bHBSS containing 18.5–37.0 kBq/ml (0.5–1 μCi/ml) of ^{211}At or 37.0–74 kBq/ml (1.0–2.0 μCi/ml) of ^{125}I, ^{123}I or $^{99m}TcO_4^-$ and with additions of NaI or $NaClO_4$ as given in the Results section. After 1 h or at the indicated times the medium was completely removed and the cells were quickly washed twice with 1 ml of ice-cold bHBSS. Cellular radioactivity was released with 1 ml of ice-cold ethanol for 20 min and counted in a cross-calibrated gamma-counter. The protein content of three to six wells per cell line was determined using a BCA assay kit (Pierce, Rockford, Ill., USA) following lysis of the residue in 0.1 *M* NaOH. For sodium-dependent radionuclide uptake, NaCl concentrations in the incubation buffer were varied by iso-osmotic substitution using choline chloride.

For efflux measurements, cells grown in 35-mm plates were incubated with the indicated radionuclide for 1 h as described above. Following medium removal and two rapid washes with ice-cold bHBSS, cells were incubated with bHBSS at 37°C. The buffer was repeatedly replaced with bHBSS at various times up to 90 min, and the radioactivity of the removed medium was determined in the same counter as mentioned above. Finally, residual radioactivity was extracted with ethanol and measured. The cellular uptake at the start of the efflux experiment calculated by summation of radioactivity in the media and in the cell extract was set to 100%, and results were expressed as the fraction of remaining cellular radioactivity for each time point.

All activity data were corrected for decay and normalized to protein content. Data of in vitro experiments are from one representative experiment out of one to three independent replications, each performed in triplicate. Results are given as mean values±SD.

Xenotransplantation and radionuclide uptake in vivo. Animal experiments were performed according to the German federal laws relating to the conduct of animal experimentation and to the Institutional Animal Care and Use Committee guidelines of Medizinische Hochschule Hannover. NMRI nu/nu nude mice were maintained under specific pathogen-free conditions with free access to water and rodent chow. Thyroid blocking protocols were not used at all. Xenotransplants derived from K1 were established in nude mice aged 3–4 weeks by s.c. injection of 7.5×10^6 cells/0.3 ml phosphate-buffered saline (K1-NIS: right flank; K1 wt: left flank). Subcutaneous K1 and K1-NIS tumours were easily identified and the tumour diameters were determined by using a calliper rule. The tumour volume was estimated by using the formula: length (mm) × width (mm) × height (mm) × 0.52 [31]. After 3–4 weeks of tumour growth, maximum diameters of all tumours ranged between 10 and 12 mm. At this time in vivo studies were performed. One, 3 and 24 h after i.p. injection of 2.0 MBq $Na^{123}I$ (day 1), 10.0 MBq $^{99m}TcO_4^-$ (day 2) or 0.4 MBq $Na^{211}At$ (day 4) the tumour uptake of different radionuclides in vivo was evaluated by using a ZLC370 gamma camera system (Siemens) with a LEAP collimator. Animals were placed directly onto the collimator. Higher amounts of $Na^{123}I$ and $^{99m}TcO_4^-$ compared with ^{211}At were used to achieve good image quality. No therapeutic or stunning effects of these gamma-emitters were expected. ^{211}At was applied at

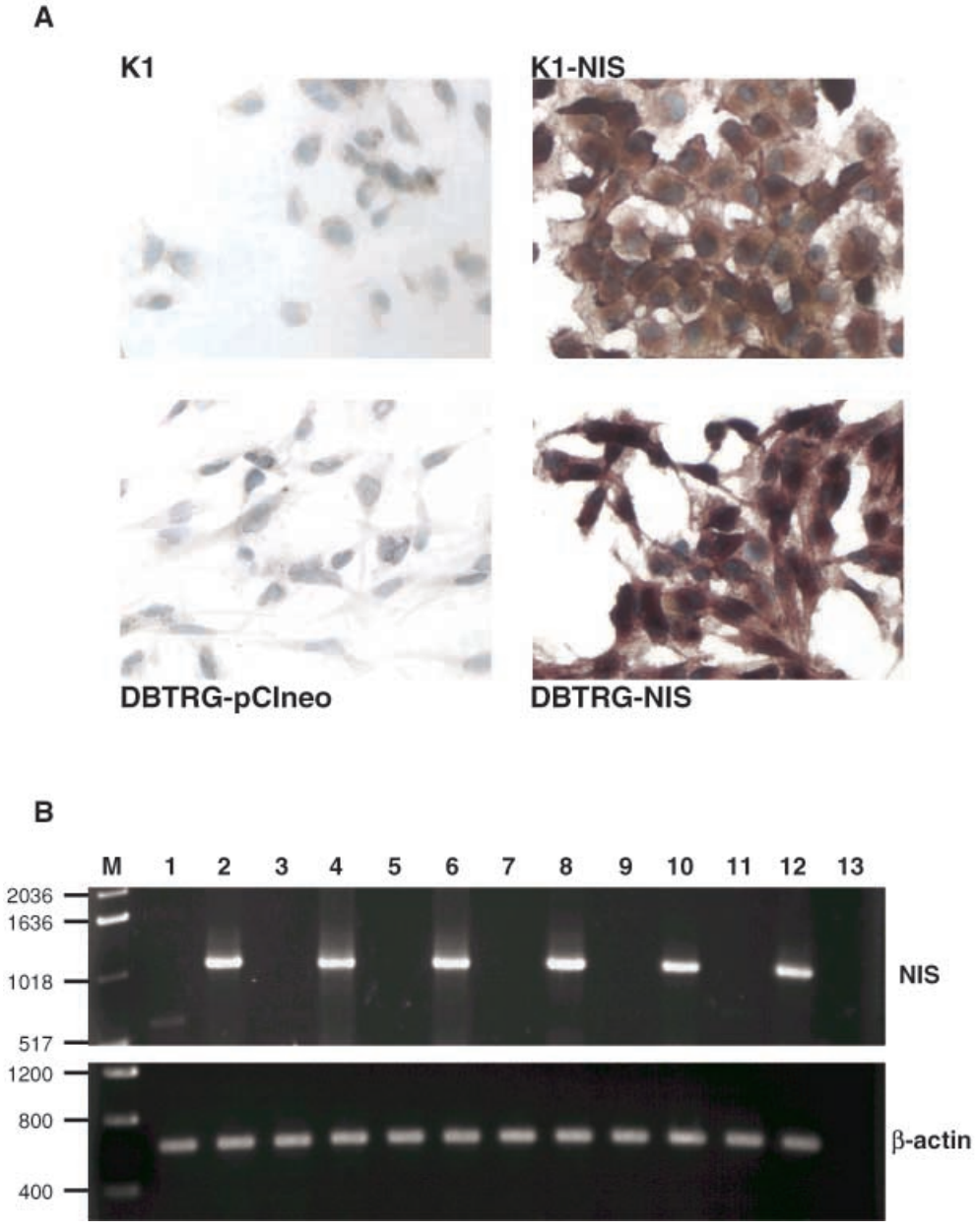

Fig. 1A, B. NIS expression in cell lines. **A** K1, K1-NIS, DBTRG-pCIneo and DBTRG-NIS cells were immunostained using a purified NIS-specific rabbit antibody and visualized by peroxidase reaction using DAB as chromogen (brown colour) followed by nuclear counterstaining with haematoxylin (blue colour). **B** Equal amounts of total RNA were reverse transcribed and subjected to PCR with NIS-specific primers (*upper panel*, expected product size 1,021 bp) or β-actin-specific primers (*lower panel*, expected product size 621 bp). PCR products were separated by agarose gel electrophoresis and stained with ethidium bromide. Lanes 2, 4, 6, 8, 10 and 12 correspond to stable NIS-transfected cells K1, B-CPAP, 8505-C, SW480, CACO-2 and DBTRG, respectively. Lanes 1, 3, 5, 7, 9 and 11 correspond to the respective parental (K1 and 8505-C) or pCIneo-transfected control cell lines. In both parts of B, lane 13 includes negative controls for PCR (no template added). Figures on the *left* indicate the size (in bp) of DNA markers applied in Lanes M

Table 1. Human cell lines used in this study

Cell line	Tumour origin	Supplier/code	Ref.
K1	Papillary thyroid carcinoma	ECACC/92030501	[52]
B-CPAP	Papillary thyroid carcinoma	DSMZ/ACC273	[53]
8505-C	Undifferentiated thyroid carcinoma	DSMZ/ACC219	[54]
SW480	Colon adenocarcinoma	DSMZ/ACC313	[55]
CACO-2	Colon adenocarcinoma	DSMZ/ACC169	[56]
DBTRG-05MG	Glioblastoma	DSMZ/ACC359	[57]

the end to avoid possible damaging effects leading to interference with $Na^{123}I/^{99m}TcO_4^-$ scintigraphy. Images were acquired with Micro Dot Imager (Siemens) within 5- to 10-min periods (in total 100,000 counts) at radionuclide-specific γ-energy peaks (159 keV for ^{123}I, 140 keV for ^{99m}Tc, 81 keV for ^{211}At) using a window width of 15%. For preliminary organ distribution analysis, three adjacent circular regions of interest (ROIs) with a diameter of 5 mm were placed in the centre of the organ of interest in each animal (n=3). The count data were background subtracted and converted without recovery correction to K1-NIS tumour to non-tumour ratios (i.e. ratio of average counts as mean±SD; n=3). No correction methods for attenuation or scatter were applied because

the animals were placed directly onto the collimator with a small distance (<5 mm) between the collimator and the tumour.

Dosimetry. From the scintigraphy data obtained for ^{123}I and ^{211}At at 1 h, 3 h and 24 h post injection, preliminary dosimetric calculations were performed according to the MIRD concept in K1-NIS tumour-bearing nude mice (n=2). Data were background subtracted and converted to activity values (MBq) by calibrating the gamma camera system with defined activities. No corrections were made for scatter, attenuation and recovery. Data were fitted to a mono-exponential elimination function [$y=A\cdot e^{-Bt}$ with A= maximum activity, B= effective elimination constant, y= retained activity (MBq), and t= time (h)] using a spreadsheet program. Effective elimination constants were used to calculate the effective half lives of ^{211}At and ^{123}I. The biological half-life (T_{biol}) of ^{123}I calculated from effective (T_{eff}) and physical half-lives (T_{phys}) was used to estimate the effective half-life of ^{131}I ($1/T_{eff}=1/T_{biol}+1/T_{phys}$). Maximum tumour activities were estimated at 3 h post injection. Decay data in the MIRD format (National Nuclear Data Center at Brookhaven National Laboratory, Upton, N.Y., USA), with inclusion of α-, β-, and γ-particle, Auger electron and recoil (^{211}At) radiation, were used to calculate S values and the absorbed dose as described by Junker and Fitschen [43]:

$$D = F \cdot A \cdot S \text{ and } S = (\sum y_i \cdot E_i)/m$$

with D= mean absorbed dose value under assumption of homogeneous distribution in the tumour (Gy); F= unit conversion factor; A= cumulated tumour activity (Bq·h); y_i= yield of i^{th} decay component $(Bq\cdot s)^{-1}$; E_i= emission energy of i^{th} decay component (MeV); m= tumour mass (g).

Furthermore, tumour uptake (%) and tumour dose in Gy/MBq were calculated for both radionuclides to estimate their potential use for tumour cell kill.

Results

Human NIS cDNA was cloned in the pCIneo vector (cf. Materials and methods section) to confer constitutive NIS expression driven by the CMV promoter in recipient cells. In previous pilot studies a panel of 14 different human cell lines representing eight different tumour tissues (follicular and medullary thyroid, breast, colon, liver, kidney, prostate and brain) was modified by transient transfection with the expression construct, and $NaClO_4$-sensitive $Na^{125}I$ uptake was determined. Uptake was found to be correlated with transfection efficiencies as monitored by parallel reporter gene assays (T. Petrich and E. Pötter, unpublished data). Out of this panel, six cell lines (Table 1) were transfected with the NIS expression vector, subsequently selected by antibiotic resistance and screened for $NaClO_4$-sensitive $Na^{125}I$ uptake capacity to identify stable NIS-expressing cell culture models for further studies. To confirm NIS expression in selected cell clones following expansion and growth, immunohistochemistry with a purified rabbit antibody raised against a peptide located at the carboxy-terminal end of NIS and mRNA analysis by RT-PCR was performed. As shown for K1 and DBTRG, stable NIS-transfected cells were intensely stained using the NIS-specific

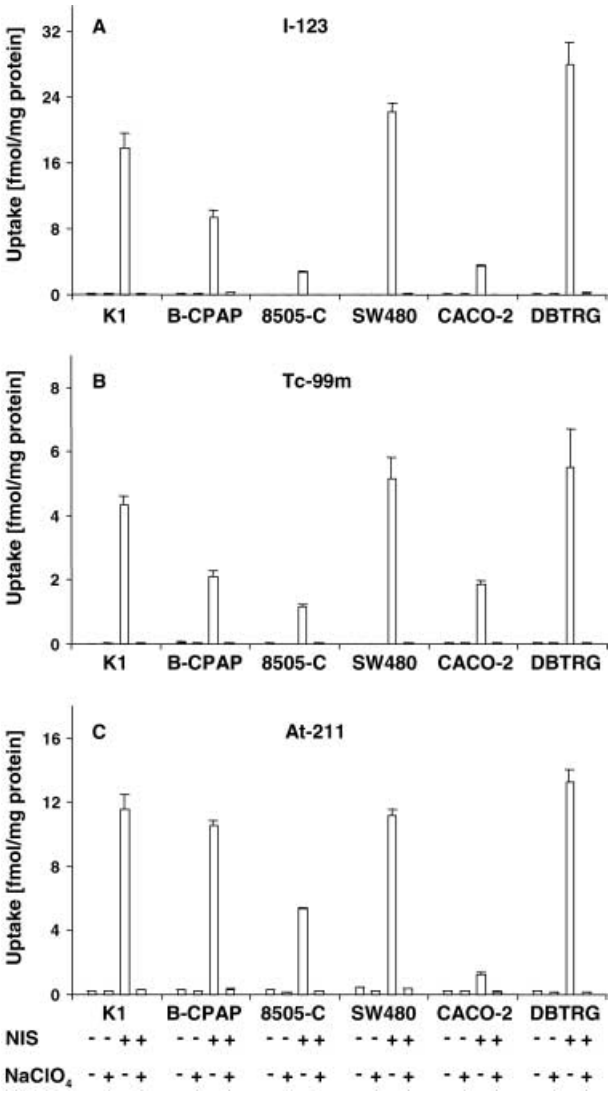

Fig. 2A–C. Comparison of NIS-dependent radionuclide uptake. Control cell lines and NIS-transfected cell lines were incubated for 1 h with ^{123}I (**A**), $^{99m}TcO_4^-$ (**B**) or ^{211}At (**C**) in the presence or absence of 150 μ*M* $NaClO_4$ (NIS-status and $NaClO_4$ treatment are indicated at the bottom of the figure by – and +). Cellular radioactivity was released with ethanol, counted and normalized to protein content. Results are mean values±SD (n=3)

antibody, in contrast to K1 parental cells and stable pCIneo-transfected DBTRG cells (Fig. 1A). Similarly, all NIS-transfected cell lines expressed high levels of NIS mRNA, as judged from semiquantitative RT-PCR of equal amounts of total RNA using NIS-specific primers (Fig. 1B, upper panel), in contrast to the respective control cell lines. Parallel RT-PCR amplification of β-actin mRNA served as a control for RNA integrity and absence of DNA contamination (Fig. 1B, lower panel), the latter of which would have resulted in an additional band in the β-actin PCR due to co-amplification of the small intron-containing genomic DNA target.

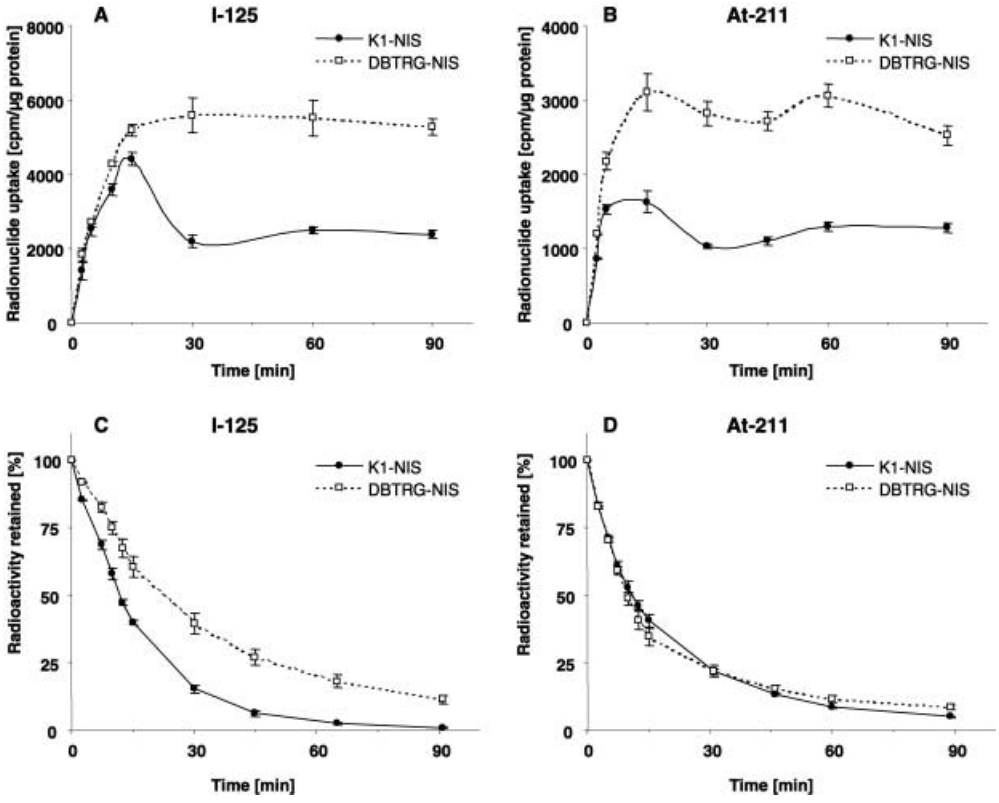

Fig. 3. Time course of radionuclide uptake (**A, B**) and release (**C, D**). NIS-expressing cell lines K1-NIS and DBTRG-NIS were incubated with **A** ^{125}I or **B** ^{211}At in the presence or absence of 150 µ*M* $NaClO_4$ for various times (2.5–90 min). Cellular radioactivity was solubilized with ethanol and normalized to protein content. Results of $NaClO_4$ inhibition for each time point were subtracted from the data to obtain NIS-specific uptake. Results are mean values±SD (*n*=3). To study efflux, cells were preloaded for 1 h (*t*=0) with **C** ^{125}I or **D** ^{211}At, followed by repeated exchange of bHBSS at various times over a period of 90 min. Cellular uptake at *t*=0 calculated by summation of radioactivity in all media and the final cell extract was set to 100%, and results were expressed as fraction of radioactivity retained by the cells for each time point. Results are mean values±SD (*n*=3)

Radionuclide uptake characteristics in vitro

Steady-state radionuclide uptake of stable NIS-expressing cell lines was compared with respective parental cells or pCIneo transfectants in the absence or presence of 150 µ*M* $NaClO_4$, an established competitive inhibitor of NIS-mediated iodide transport (Fig. 2). To obtain similar concentrations and radioactivities in these experiments, no-carrier-added $Na^{123}I$ was used instead of $Na^{125}I$ because its half-life (13.2 h) compares favourably with that of ^{211}At (7.2 h) and $^{99m}TcO_4^-$ (6.0 h). ^{211}At was applied directly (usually <2 h after cyclotron production) and most probably in the form of $Na^{211}At$ in the incubation buffer. Following 1-h incubation and cellular extraction, significant uptake of all three radionuclides ($Na^{123}I$, $^{99m}TcO_4^-$, ^{211}At) was obtained only in NIS-expressing cells in the absence of the inhibitor. In contrast, parental or pCIneo-transfected tumour cells did not accumulate radioiodide or $^{99m}TcO_4^-$, but in all control cell lines the ^{211}At uptake background was considerably higher and displayed variability, making comparison of transport capacities in terms of absolute amounts difficult. Nevertheless, the amounts of radioiodide taken up in the NIS-transfected cells after 1 h apparently exceeded those of ^{211}At and $^{99m}TcO_4^-$. The uptake values of the NIS-transfected cells ranged between 40- and 350-fold, 40- and 340-fold and 5- and 60-fold of control cell levels for $Na^{123}I$, $^{99m}TcO_4^-$ and ^{211}At, respectively. These results and the similarity of the overall uptake patterns obtained for the three radionuclides in six different NIS-expressing cell lines clearly indicate that ^{211}At uptake is an NIS-mediated process comparable to radioiodide uptake. Further evidence for the latter assumption is provided by the sensitivity of the NIS-based uptake component towards the established competitive inhibitor, $NaClO_4$: as expected, $Na^{123}I$ and $^{99m}TcO_4^-$ accumulation was completely (>98%) inhibited by 150 µ*M* $NaClO_4$ in each of the NIS tumour cell lines used (Fig. 2A, B) and ^{211}At uptake was decreased to the respective control cell levels (Fig. 2C). In addition, uptake of radioiodide and ^{211}At showed dose-dependent inhibition in K1-NIS and SW480-NIS cells in experiments performed within the range of 1–1,000 µ*M* $NaClO_4$. Two to 5 µ*M* $NaClO_4$ decreased the radioiodide and astatide uptake to 10%–20% and 30%–50%, respectively (data not shown).

The time courses of cellular radionuclide uptake and release were studied in K1-NIS and DBTRG-NIS cells

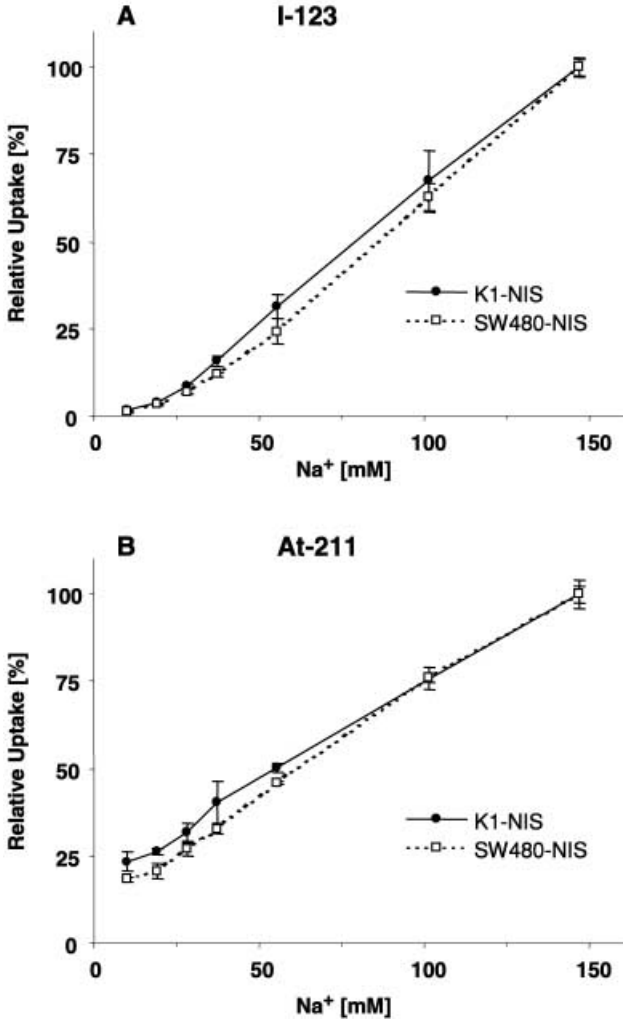

Fig. 4A, B. Na^+ dependence of radionuclide accumulation. K1-NIS and SW480-NIS cells were incubated with ^{123}I (**A**) and ^{211}At (**B**) for 1 h at various extracellular Na^+ concentrations (10–150 m*M*). Cellular radioactivity was released with ethanol, counted and normalized to protein content. Results were expressed as % of the maximum uptake value obtained for each cell line and radionuclide. Results are mean values±SD (*n*=3)

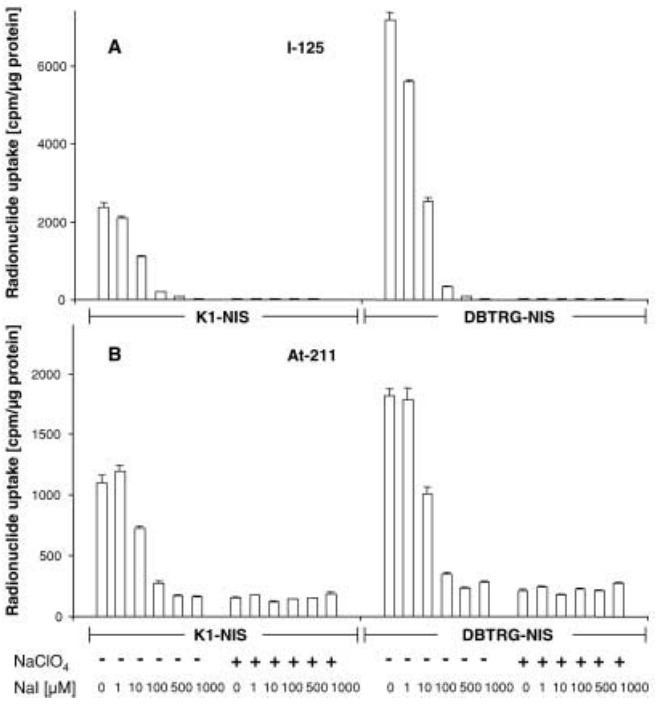

Fig. 5A, B. Effect of NaI on radionuclide accumulation. K1-NIS and DBTRG-NIS cells were incubated for 1 h with ^{125}I (**A**) or ^{211}At (**B**) with additions of unlabelled NaI and of 150 µ*M* $NaClO_4$ as indicated at the bottom of the figure. Cellular radioactivity was released as described and normalized to protein content. Results are mean values±SD (*n*=3)

for $Na^{125}I$ and ^{211}At (Fig. 3). To assess non-NIS-mediated binding in influx measurements, NIS-specific uptake in parallel wells was blocked by addition of 150 µ*M* $NaClO_4$ for all time points (2.5–90 min). This unspecific binding was subtracted to obtain NIS-specific uptake (Fig. 3A, B). Again ^{211}At uptake in the presence of $NaClO_4$ was higher compared with near-to-complete inhibition of $Na^{125}I$ uptake. Following application, rapid accumulation of both radionuclides in the two cell lines was measured, reaching half-maximum after 5–10 min and a plateau after ~30 min, indicative for balanced influx and efflux (Fig. 3A, B). The parallel time course of radioiodine and astatine, therefore, implies similar transport kinetics. After pre-loading the cells with $Na^{125}I$ or ^{211}At, efflux was studied by repeated replacement of the incubation buffer at various times over a total period of 90 min. Following determination of radioactivities of all media and of the final cell extracts, the retained cellular radioactivity was calculated for each time point. Accordingly, under conditions limiting re-uptake a fast release of both radionuclides was recorded with apparent $t_{1/2}$ of ~10–15 min for $Na^{125}I$ (Fig. 3C) and of ~7–10 min for ^{211}At (Fig. 3D). Whereas slightly different efflux curves of ^{125}I were obtained in K1-NIS, DBTRG-NIS (Fig. 3C) and SW480-NIS cells (not shown), these were not obvious for ^{211}At.

It is well known that NIS-dependent iodide uptake essentially requires extracellular Na^+ ions [2, 42, 44]. Using choline chloride as an iso-osmotic substitute for NaCl, the concentration of Na^+ ions was varied within a range of 10–150 m*M* to determine the Na^+ dependence of radionuclide accumulation (Fig. 4). As shown for K1-NIS and SW480-NIS cells, an approximately linear correlation was found between extracellular concentration of sodium and uptake of both radionuclides, ^{123}I (Fig. 4A) and ^{211}At (Fig. 4B). Whereas radioiodide uptake was completely abolished at the lowest NaCl concentration, the uptake of ^{211}At was reduced to values of only 20%–25%. This effect compares well with the non-specific uptake of the control cells. Due to the lack of a stable At isotope, no saturation kinetic data can be ob-

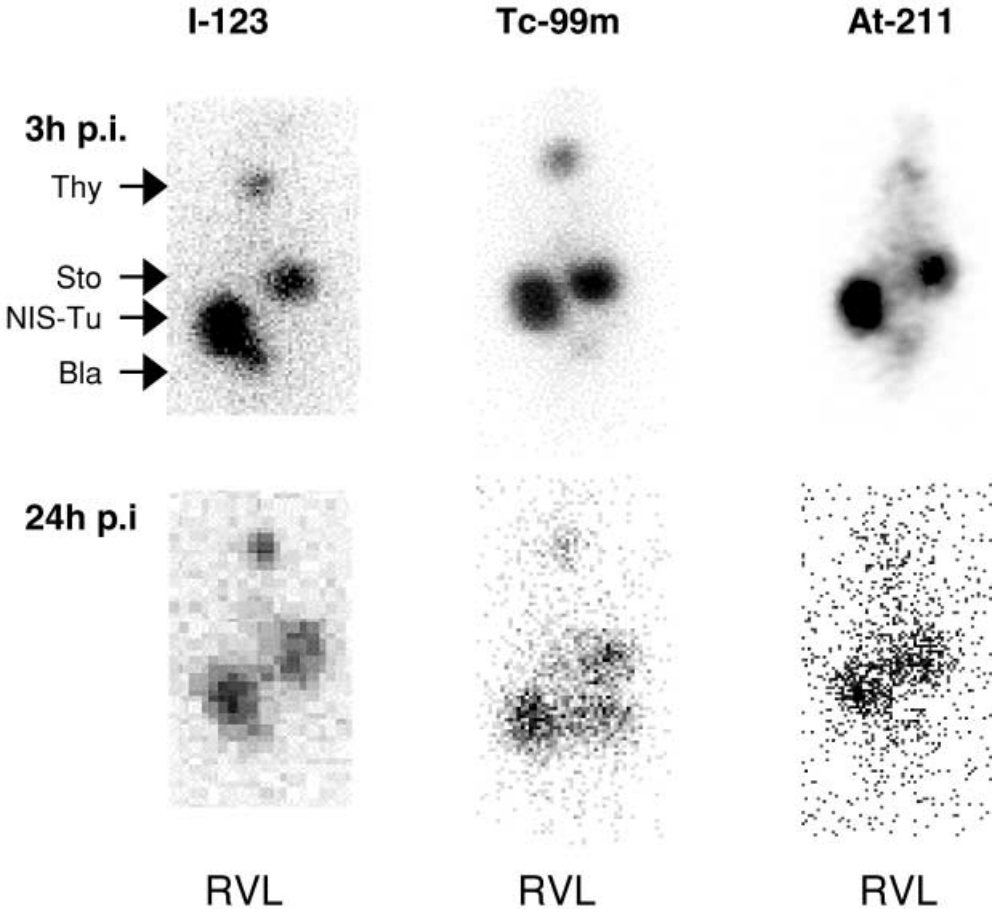

Fig. 6. Radionuclide uptake and tumour imaging in vivo. Scintigraphy of K1 and K1-NIS tumour-bearing nude mice with 2.0 MBq $Na^{123}I$, 10.0 MBq $^{99m}TcO_4^-$ and 0.4 MBq free ^{211}At at 3 h (*upper panel*) and 24 h (*lower panel*) after intraperitoneal injection in the same animal on different days (ventral view; *RVL*, right ventral left). Photon energies of 159, 140 and 81 keV were used for scintigraphy of ^{123}I, $^{99m}TcO_4^-$ and ^{211}At, respectively. Significant uptake of radionuclides in NIS tumour (*NIS-Tu*, right flank) was revealed, whereas control tumour (left flank) showed no uptake. Physiological accumulation was detected in thyroid (*Thy*), stomach (*Sto*) and bladder (*Bla*)

tained to characterize NIS-mediated ^{211}At transport. Instead, the effect of NaI concentrations on ^{211}At steady-state uptake (1 h) was determined by means of heterologous competition. As shown for K1-NIS and DBTRG-NIS cells in Fig. 5B, presence of NaI leads to decrease in ^{211}At accumulation in cells in a concentration-dependent manner, which at ~500 µ*M* NaI equals that of cells inhibited by 150 µ*M* $NaClO_4$ (Fig. 5B) or respective control cells (data not shown). In addition, the pattern obtained was quite similar to that in analogous experiments performed with ^{125}I, in which, however, NaI caused a greater decrease in steady-state ^{125}I uptake (Fig. 5A).

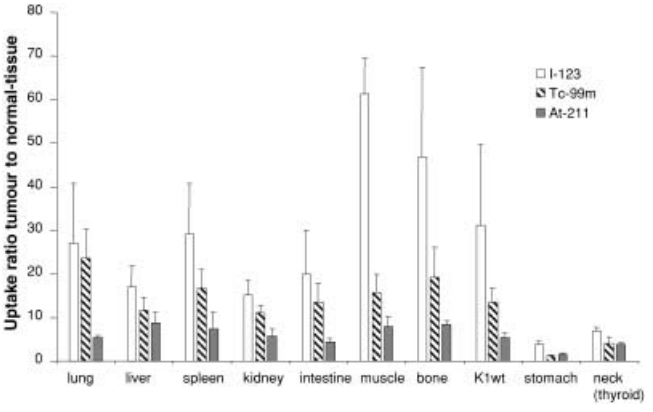

Fig. 7. Biodistribution. K1-NIS tumour to normal tissue (or to control K1 tumour) ratios 3 h after intraperitoneal injection evaluated by scintigraphy. High ratios were found in all regions, except the stomach and the neck region which included the thyroid

Radionuclide uptake and biodistribution in vivo

To evaluate radioiodine and astatine uptake in vivo, a papillary thyroid carcinoma xenograft was established in nude mice using parental K1 and K1-NIS cells transplanted into the left and the right flank, respectively. After tumour growth for 3–4 weeks, scintigraphy was performed with 2.0 MBq ^{123}I, 10.0 MBq $^{99m}TcO_4^-$ and 0.4 MBq ^{211}At 3 and 24 h after i.p. injection in the same animal on different days (Fig. 6) without visible intermediate tumour growth during an imaging period of a maximum of 4 days. The K1-NIS-derived tumour displayed radionuclide uptake at least one order of magnitude greater than the control tumour (left flank) or most normal tissues as judged from biodistribution evaluated by scintigraphy and ROI analysis (Fig. 7). In addition to bladder uptake, significant physiological uptake was found in the stomach and thyroid. The tumour to non-tumour count ratios were lower after injection of ^{211}At than

Table 2. Dosimetric calculation (MIRD) for ^{131}I and ^{211}At (Example of two K1-NIS tumour-bearing mice)

	^{123}I (^{131}I)		^{211}At	
	Mouse I	Mouse II	Mouse I	Mouse II
Tumour volume (ml)	0.65	0.52	0.65	0.52
Elimination function[a]	$y=0.4881e^{-0.1018t}$	$y=0.2254e^{-0.1142t}$	$y=0.0584e^{-0.1273t}$	$y=0.0731e^{-0.142t}$
Physical half-life (h)	13.2 (193)	13.2 (193)	7.2	7.2
Effective half-life (h)	6.8, (13.1[c])	6.1, (10.7[c])	5.4	4.9
Biological half-life (h)	14.0	11.3	21.6	15.3
Total applied activity (MBq)	0.670	1.130	0.643	0.619
Tumour activity (MBq)[b]	0.360	0.160	0.075	0.097
Tumour uptake (%)[b]	53.7	14.2	11.6	15.7
Tumour dose (Gy)	1.25[c]	0.57[c]	3.54	5.12
Dose factor (Gy/MBq$_{tumour}$)	3.49[c]	3.54[c]	47.34	53.33
Dose factor (Gy/MBq$_{total}$)	1.88[c]	0.50[c]	5.50	8.36

[a] t= time (h), y= tumour activity (MBq)
[b] T_{max}=3 h after injection
[c] Calculation for ^{131}I based on in vivo data of ^{123}I

after injection of Na^{123}I or $^{99m}TcO_4^-$. To avoid higher scatter effects, ROIs were placed in the centre of the organ of interest with a minimum distance of 10 mm to hot lesions (bladder and stomach).

Dosimetry

Calculations were performed in two animals with tumour volumes of 0.65 ml (mouse I) and 0.52 ml (mouse II) at the time of radionuclide administration and scintigraphy (Table 2). Preliminary dosimetric calculations (MIRD) for intracellular uptake of radionuclides were obtained assuming tumour characteristics of spherical form, density of 1 g/ml and homogeneous radionuclide distribution. Elimination functions were obtained by fitting acquired time-activity curves for both ^{123}I and ^{211}At [t=time (h), y= tumour activity (MBq)]. Biological half-lives and T_{max} (=3 h) in tumours of ^{211}At and iodine isotopes did not show great differences. According to differences in physical $T_{1/2}$, effective half-lives of ^{131}I were longer than those of ^{211}At (Table 2). Using ^{131}I for calculations, the tumour-related dose factor was considerably lower compared with ^{211}At (3.49 and 3.54 Gy/MBq vs 47.34 and 53.33 Gy/MBq in mice I and II; Table 2).

Discussion

Efforts to use the NIS gene for experimental tumour therapy by means of gene transfer coupled with conventional radioiodine therapy have been given tremendous impetus by its molecular identification just 5 years ago [2]. This is reflected in the increasing number of related studies, including this work, aimed at elucidating NIS-mediated transport and evaluating alternative means of cancer therapy [26, 27, 28, 29, 30, 31, 32, 33, 34, 35]. While basic problems inherent in somatic gene therapy strategies, including safety and specific and complete gene delivery to target cells, remain to be solved, several reports indicate that transfer of expression constructs carrying the NIS gene fused to strong promoters is sufficient to restore iodide uptake in thyroid cell lines [26, 33, this work] or to induce de novo high iodide uptake capacity in various non-thyroidal tumour cell lines, making recipient cells sensitive to radioiodine therapy, at least in vitro [26, 27, 29, 32, 34, this work]. Furthermore, in the LNCaP prostate cancer model, tissue-specific and androgen-inducible NIS expression has been achieved using the prostate-specific antigen promoter [30], and tumours of stable NIS-transfected LNCaP cells grown in athymic nude mice have been successfully eradicated by Na^{131}I [31]. Although extraordinarily high activities (111 MBq) were applied in the latter study, it provided encouraging proof-of-principle data for effective NIS-based therapy in a prostate-derived tumour model lacking expression of thyroid-specific genes, i.e. TPO and TG, as a prerequisite for iodide organification. Unfortunately, most studies report rapid leakage of radioiodide in NIS-modified cells following uptake, which, although leading to cell kill in vitro, prevents therapeutically effective doses from being reached in vivo [26, 27, 29, 32, 34, 35].

In this study we explored an alternative route for NIS-mediated strategies using the halide ^{211}At. This is regarded as a promising radionuclide for cell-targeted radiotherapy owing to a combination of favourable properties, including short half-life (7.2 h) and decay via a bi-branch pathway emitting two α-particle types (6.8 MeV mean energy), leading to deposition of high energy over a short distance (55–88 µm mean tissue range). Several ^{211}At-labelled compounds have been generated and char-

acterized for future prospective treatments, e.g. tumour-directed monoclonal antibodies, *meta*-iodobenzylguanine analogues, colloids and methylene blue [for reviews see 45, 46, 47].

We established six modified cell culture working models for papillary (K1-NIS, B-CPAP-NIS) and anaplastic (8505-C-NIS) thyroid carcinoma, colon carcinoma (SW480-NIS, CACO-2-NIS) and glioblastoma (DBTRG-NIS), which were proven to express human NIS (Fig. 1) and accordingly accumulate radioiodide in the range of ~40- to 350-fold compared with control cells (Fig. 2), which is in general agreement with reports on other cell lines invoking rat [2, 25, 26, 27, 28, 32] or human [3, 29, 33, 34, 35, 36] NIS constructs.

Our data obtained in vitro provide sufficient direct evidence that the NIS is capable of transporting ^{211}At with characteristics very similar to that of its physiological substrate, iodide. This conclusion can clearly be drawn when results are considered in combination (cf. Figs. 2, 3, 4, 5). These results can be briefly summarized as follows: The time courses of uptake and release were similar for ^{211}At and radioiodide. NIS expression was accompanied by a 10- to 50-fold increase in ^{211}At accumulation compared with control cells, which could be abolished by $NaClO_4$, by decreasing the extracellular Na^+ concentration and by competition with iodide. Considering that higher absolute amounts of radioiodide than of ^{211}At were applied (because of their different physical half-lives) and that uptake is almost linearly correlated with applied radioactivity in this range (data not shown), radioiodide and ^{211}At uptake capacity are in the same order of magnitude in NIS-expressing cells. On the other hand, all NIS-negative control cells displayed varying levels of non-$NaClO_4$-sensitive ^{211}At uptake throughout the study, which were always found to be considerably higher than in parallel studies using no-carrier-added forms of ^{123}I, ^{125}I and $^{99m}TcO_4^-$. Therefore, quantification in absolute terms appears questionable. This does not contradict one of the main conclusions, i.e. NIS directly transports ^{211}At, as shown in Figs. 2, 3, 4, 5 and 6, but may indicate that alternative low-capacity ^{211}At uptake pathways exist in different cell types, e.g. via other carrier systems. Other explanations for the observed phenomena include unspecific adsorption processes to the plasma membrane lipid bilayer and to free plastic surfaces, which were occasionally detected and could be decreased by pre-coating with serum, but were in general difficult to control owing to in-Lot and Lot-to-Lot variations (data not shown). Moreover, in solutions at near-to-neutral pH, as used here, ^{211}At can adopt different chemical forms that, apart from astatide, may include monovalent oxyanions [see 48, and references therein]; these forms can be predicted to differ both in adsorption properties and, more importantly, in NIS-mediated transport or binding characteristics. Regarding NIS-based transport, given NIS' broad substrate selectivity it is tempting to speculate that a similar situation may exist for ^{211}At's monovalent anion species as is already known for other halides; for example, I^- and ClO_3^- are better NIS substrates than IO_4^-, and ClO_4^- binds but is not transported [7, 49, 50]. We tried to account for these unknowns by including Na_2SO_3 to keep ^{211}At in a reduced state (i.e. astatide) following dry distillation. However, to more directly identify the species involved, adequate analytical methods not available so far will have to be established and applied.

Our cell culture data are in agreement with results recently published by Lindencrona et al. [40]. These authors compared transport of ^{211}At and radioiodide in pig thyrocytes cultured in a bicameral system, which, in contrast to this work on monolayer cells, allowed bidirectional transcellular fluxes to be studied in polarized cells [40]. Even though NIS was not studied directly, equivalent conclusions were derived concerning NIS-mediated and NIS-independent ^{211}At cellular transport routes, and the study of Lindencrona et al. thus nicely complements our own work in major respects.

Using K1 cells we established the first xenograft athymic nude mouse model for papillary thyroid cancer with and without NIS expression. Whereas cell culture experiments showed high specificity of intracellular transport by NIS for radioiodine, ^{211}At and $^{99m}TcO_4^-$, the in vivo experiments suggest that there are significant differences between these three agents, with ^{211}At being less selectively accumulated in K1-NIS-derived tumours (Fig. 7). As already discussed, this may relate to alternative routes bypassing NIS-mediated ^{211}At transport. The pertinent data, however, concern the number of counts within the respective ROIs. Due to the high energy of photons emitted by ^{211}At in addition to the 81-keV photons used for scintigraphy, an inferior point spread function may be assumed, but appropriate phantom studies have not been performed. Yet, the ratios of count densities measured in tumour and non-tumour tissue ranged between 5 and 10.

Apart from target selectivity, radiosensitivity of tumours and the emission properties of the applied isotope, radionuclide therapy is governed by two major factors that decide the tumouricidal potential, namely the effectiveness of intracellular transport and the mean intracellular residence time, related to the physical half-life of the radionuclide and its cellular retention. Regarding the kinetics of radioiodine and ^{211}At, cell culture experiments showed similar efflux rates, with half-lives in the range of 3–15 min depending on the cell line; this is in agreement with previous reports obtained for radiodide [26, 27, 28, 29, 33, 34, 35, 42]. The situation in vivo, however, is apparently different, with biological half-lives of about 13–18 h for both halides (Table 2), indicating that there is continuing re-uptake from blood that compensates for cellular efflux, in contrast to the wash-out conditions in vitro that limit re-uptake. Consequently, 3 h p.i., imaging still shows intense activity accumulation by NIS tumours, which even after 24 h are positively contrasted (Fig. 6).

The in vivo uptake of ^{123}I by the NIS-derived tumours observed in this study is higher than that reported by other investigators [35]. Differences may in part reflect the presence of other proteins determining retention and efflux, e.g. pendrin [51], which represent important pharmacological targets to improve cellular retention. Accordingly, it can be assumed that, upon NIS modification, certain tumour types retain radioiodine for longer than others.

With the exception of the study by Spitzweg et al. [31], previous reports have shown a short effective half-life of ^{131}I or low-energy doses in xenografts [26, 28, 32, 35]. By contrast, according to preliminary dosimetric calculations, the radioiodine kinetics obtained in this study in vivo would allow the treatment of NIS tumours with $Na^{131}I$. The calculation for ^{211}At, however, results in doses that are higher by a factor of 5 per administered activity than for ^{131}I. The consequences for tumour remission, including possible side-effects on other organs, will be investigated in further work.

It is concluded that ^{211}At is efficiently transported by NIS, that the retention time in experimental NIS-modified tumours in vivo is adequate in relation to the 7-h half-life of the nuclide, and that tumouricidal doses might be achieved. ^{211}At, which shows kinetics in NIS-transfected cells similar to those of radioiodine, may be more appropriate for NIS-mediated tumour therapy than ^{131}I.

Acknowledgements. The authors thank Mrs. Z. Korkmaz for excellent technical assistance and Drs. J. Fitschen and H.W. Tiffe for advice on dosimetric calculations. We are very grateful to Dr. J.C. Morris (Mayo Clinic, Rochester, Minn., USA) for the generous gift of an NIS-specific control antibody.

References

1. Mazzaferri EL. Radioiodine and other treatment and outcomes. In: Braverman LE, Utiger RD, eds. *Werner & Ingbars The Thyroid.* Philadelphia: Lippincott Williams and Wilkins, 2000.
2. Dai G, Levy O, Carrasco N. Cloning and characterization of the thyroid iodide transporter. *Nature* 1996; 379:458–460.
3. Smanik PA, Liu Q, Furminger TL, Ryu K, Xing S, Mazzaferri EL, Jhiang SM. Cloning of the human sodium iodide symporter. *Biochem Biophys Res Commun* 1996; 226:339–345.
4. Smanik PA, Ryu KY, Theil KS, Mazzaferri EL, Jhiang SM. Expression, exon-intron organization, and chromosome mapping of the human sodium iodide symporter. *Endocrinology* 1997; 138:3555–3558.
5. Perron B, Rodriguez AM, Leblanc G, Pourcher T. Cloning of the mouse sodium iodide symporter and its expression in the mammary gland and other tissues. *J Endocrinol* 2001; 170:185–196.
6. Carrasco N. Iodide transport in the thyroid gland. *Biochim Biophys Acta* 1993; 1154:65–82.
7. De La Vieja A, Dohan O, Levy O, Carrasco N. Molecular analysis of the sodium/iodide symporter: impact on thyroid and extrathyroid pathophysiology. *Physiol Rev* 2000; 80: 1083–1105.
8. Spitzweg C, Joba W, Eisenmenger W, Heufelder AE. Analysis of human sodium iodide symporter gene expression in extrathyroidal tissues and cloning of its complementary deoxyribonucleic acids from salivary gland, mammary gland, and gastric mucosa. *J Clin Endocrinol Metab* 1998; 83:1746–1751.
9. Vayre L, Sabourin JC, Caillou B, Ducreux M, Schlumberger M, Bidart JM. Immunohistochemical analysis of Na^+/I^- symporter distribution in human extra-thyroidal tissues. *Eur J Endocrinol* 1999; 141:382–386.
10. Tazebay UH, Wapnir IL, Levy O, Dohan O, Zuckier LS, Zhao QH, Deng HF, Amenta PS, Fineberg S, Pestell RG, Carrasco N. The mammary gland iodide transporter is expressed during lactation and in breast cancer. *Nat Med* 2000; 6:871–878.
11. Spitzweg C, Dutton CM, Castro MR, Bergert ER, Goellner JR, Heufelder AE, Morris JC. Expression of the sodium iodide symporter in human kidney. *Kidney Int* 2001; 59:1013–1023.
12. Petrich T, Widjaja A, Musholt TJ, Hofmann M, Brunkhorst T, Ehrenheim C, Oetting G, Knapp WH. Outcome after radioiodine therapy in 107 patients with differentiated thyroid carcinoma and initial bone metastases: side-effects and influence of age. *Eur J Nucl Med* 2001; 28:203–208.
13. Caillou B, Troalen F, Baudin E, Talbot M, Filetti S, Schlumberger M, Bidart JM. Na^+/I^- symporter distribution in human thyroid tissues: an immunohistochemical study. *J Clin Endocrinol Metab* 1998; 83:4102–4106.
14. Arturi F, Russo D, Schlumberger M, du Villard JA, Caillou B, Vigneri P, Wicker R, Chiefari E, Suarez HG, Filetti S. Iodide symporter gene expression in human thyroid tumors. *J Clin Endocrinol Metab* 1998; 83:2493–2496.
15. Filetti S, Bidart JM, Arturi F, Caillou B, Russo D, Schlumberger M. Sodium/iodide symporter: a key transport system in thyroid cancer cell metabolism. *Eur J Endocrinol* 1999; 141:443–457.
16. Ringel MD, Anderson J, Souza SL, Burch HB, Tambascia M, Shriver CD, Tuttle RM. Expression of the sodium iodide symporter and thyroglobulin genes are reduced in papillary thyroid cancer. *Mod Pathol* 2001; 14:289–296.
17. Min JJ, Chung JK, Lee YJ, Jeong JM, Lee DS, Jang JJ, Lee MC, Cho BY. Relationship between expression of the sodium/iodide symporter and ^{131}I uptake in recurrent lesions of differentiated thyroid carcinoma. *Eur J Nucl Med* 2001; 28: 639–645.
18. Dohan O, Baloch Z, Banrevi Z, Livolsi V, Carrasco N. Rapid communication: predominant intracellular overexpression of the Na(+)/I(-) symporter (NIS) in a large sampling of thyroid cancer cases. *J Clin Endocrinol Metab* 2001; 86:2697–2700.
19. Schmutzler C, Winzer R, Meissner-Weigl J, Kohrle J. Retinoic acid increases sodium/iodide symporter mRNA levels in human thyroid cancer cell lines and suppresses expression of functional symporter in nontransformed FRTL-5 rat thyroid cells. *Biochem Biophys Res Commun* 1997; 240:832–838.
20. Russo D, Manole D, Arturi F, Suarez HG, Schlumberger M, Filetti S, Derwahl M. Absence of sodium/iodide symporter gene mutations in differentiated human thyroid carcinomas. *Thyroid* 2001; 11:37–39.
21. Kogai T, Hershman JM, Motomura K, Endo T, Onaya T, Brent GA. Differential regulation of the human sodium/iodide symporter gene promoter in papillary thyroid carcinoma cell lines and normal thyroid cells. *Endocrinology* 2001; 142:3369–3379.

22. Venkataraman GM, Yatin M, Marcinek R, Ain KB. Restoration of iodide uptake in dedifferentiated thyroid carcinoma: relationship to human Na^+/I^- symporter gene methylation status. *J Clin Endocrinol Metab* 1999; 84:2449–2457.
23. Kitazono M, Robey R, Zhan Z, Sarlis NJ, Skarulis MC, Aikou T, Bates S, Fojo T. Low concentrations of the histone deacetylase inhibitor, depsipeptide (FR901228), increase expression of the Na(+)/I(-) symporter and iodine accumulation in poorly differentiated thyroid carcinoma cells. *J Clin Endocrinol Metab* 2001; 86:3430–3435.
24. Schmutzler C, Koehrle J. Innovative strategies for the treatment of thyroid cancer. *Eur J Endocrinol* 2000; 143: 15–24.
25. Kosugi S, Sasaki N, Hai N, Sugawa H, Aoki N, Shigemasa C, Mori T, Yoshida A. Establishment and characterization of a Chinese hamster ovary cell line, CHO-4J, stably expressing a number of Na^+/I^- symporters. *Biochem Biophys Res Commun* 1996; 227:94–101.
26. Shimura H, Haraguchi K, Miyazaki A, Endo T, Onaya T. Iodide uptake and experimental ^{131}I therapy in transplanted undifferentiated thyroid cancer cells expressing the Na^+/I^- symporter gene. *Endocrinology* 1997; 138:4493–4496.
27. Mandell RB, Mandell LZ, Link CJ Jr. Radioisotope concentrator gene therapy using the sodium/iodide symporter gene. *Cancer Res* 1999; 59:661–668.
28. Nakamoto Y, Saga T, Misaki T, Kobayashi H, Sato N, Ishimori T, Kosugi S, Sakahara H, Konishi J. Establishment and characterization of a breast cancer cell line expressing Na^+/I^- symporters for radioiodide concentrator gene therapy. *J Nucl Med* 2000; 41:1898–1904.
29. Cho JY, Xing S, Liu X, Buckwalter TL, Hwa L, Sferra TJ, Chiu IM, Jhiang SM. Expression and activity of human Na^+/I^- symporter in human glioma cells by adenovirus-mediated gene delivery. *Gene Ther* 2000; 7:740–749.
30. Spitzweg C, Zhang S, Bergert ER, Castro MR, McIver B, Heufelder AE, Tindall DJ, Young CY, Morris JC. Prostate-specific antigen (PSA) promoter-driven androgen-inducible expression of sodium iodide symporter in prostate cancer cell lines. *Cancer Res* 1999; 59:2136–2141.
31. Spitzweg C, O'Connor MK, Bergert ER, Tindall DJ, Young CY, Morris JC. Treatment of prostate cancer by radioiodine therapy after tissue-specific expression of the sodium iodide symporter. *Cancer Res* 2000; 60:6526–6530.
32. Boland A, Ricard M, Opolon P, Bidart JM, Yeh P, Filetti S, Schlumberger M, Perricaudet M. Adenovirus-mediated transfer of the thyroid sodium/iodide symporter gene into tumors for a targeted radiotherapy. *Cancer Res* 2000; 60: 3484–3492.
33. Smit JW, Shroder-van der Elst JP, Karperien M, Que I, van der Pluijm G, Goslings B, Romijn JA, van der Heide D. Reestablishment of in vitro and in vivo iodide uptake by transfection of the human sodium iodide symporter (hNIS) in a hNIS defective human thyroid carcinoma cell line. *Thyroid* 2000; 10: 939–943.
34. Carlin S, Cunningham SH, Boyd M, McCluskey AG, Mairs RJ. Experimental targeted radioiodide therapy following transfection of the sodium iodide symporter gene: effect on clonogenicity in both two-and three-dimensional models. *Cancer Gene Ther* 2000; 7:1529–1536.
35. Haberkorn U, Henze M, Altmann A, Jiang S, Morr I, Mahmut M, Peschke P, Kubler W, Debus J, Eisenhut M. Transfer of the human NaI symporter gene enhances iodide uptake in hepatoma cells. *J Nucl Med* 2001; 42:317–325.
36. Pohlenz J, Duprez L, Weiss RE, Vassart G, Refetoff S, Costagliola S. Failure of membrane targeting causes the functional defect of two mutant sodium iodide symporters. *J Clin Endocrinol Metab* 2000; 85:2366–2369.
37. Corson DE, MacKenzie KK, Segre E. Artificially radioactive element 85. *Phys Rev* 1940; 58:672–678.
38. Cobb LM, Harrison A, Butler SA. Toxicity of astatine-211 in the mouse. *Hum Toxicol* 1988; 7:529–534.
39. Garg PK, Harrison CL, Zalutsky MR. Comparative tissue distribution in mice of the alpha-emitter ^{211}At and ^{131}I as labels of a monoclonal antibody and F(ab')2 fragment. *Cancer Res* 1990; 50:3514–3520.
40. Lindencrona U, Nilsson M, Forssell-Aronsson E. Similarities and differences between free ^{211}At and ^{125}I transport in porcine thyroid epithelial cells cultured in bicameral chambers. *Nucl Med Biol* 2001; 28:41–50.
41. Castro MR, Bergert ER, Beito TG, McIver B, Goellner JR, Morris JC. Development of monoclonal antibodies against the human sodium iodide symporter: immunohistochemical characterization of this protein in thyroid cells. *J Clin Endocrinol Metab* 1999; 84:2957–2962.
42. Weiss SJ, Philp NJ, Grollman EF. Iodide transport in a continuous line of cultured cells from rat thyroid. *Endocrinology* 1984; 114:1090–1098.
43. Junker D, Fitschen J. Dosimetrie inkorporierter Strahler. In: Diethelm L, Heuck F, Olsson O, Vieten H, Zuppinger A, eds. *Nuklearmedizin: Radiopharmaka, Gerätetechnik, Strahlenschutz. XV*. Berlin Heidelberg New York: Springer; 1980:425–482.
44. Eskandari S, Loo DD, Dai G, Levy O, Wright EM, Carrasco N. Thyroid Na^+/I^- symporter. Mechanism, stoichiometry, and specificity. *J Biol Chem* 1997; 272:27230–27238.
45. Vaidyanathan G, Zalutsky MR. Targeted therapy using alpha emitters. *Phys Med Biol* 1996; 41:1915–1931.
46. Zalutsky MR, Vaidyanathan G. Astatine-211-labeled radiotherapeutics: an emerging approach to targeted alpha-particle radiotherapy. *Curr Pharm Des* 2000; 6:1433–1455.
47. McDevitt MR, Sgouros G, Finn RD, Humm JL, Jurcic JG, Larson SM, Scheinberg DA. Radioimmunotherapy with alpha-emitting nuclides. *Eur J Nucl Med* 1998; 25:1341–1351.
48. Berei K, Vasaros L. Recent advances in the organic chemistry of astatine. In Patai S, Rappoport Z, eds. *The chemistry of halides, pseudo-halides and azides. Supplement D2*. West Sussex: John Wiley; 1995:787–819.
49. Eskandari S, Loo DD, Dai G, Levy O, Wright EM, Carrasco N. Thyroid Na^+/I^- symporter. Mechanism, stoichiometry, and specificity. *J Biol Chem* 1997; 272:27230–27238.
50. Yoshida A, Sasaki N, Mori A, Taniguchi S, Mitani Y, Ueta Y, Hattori K, Sato R, Hisatome I, Mori T, Shigemasa C, Kosugi S. Different electrophysiological character of I^-, ClO_4^-, and SCN^- in the transport by Na^+/I^- symporter. *Biochem Biophys Res Commun* 1997; 231:731–734.
51. Royaux IE, Suzuki K, Mori A, Katoh R, Everett LA, Kohn LD, Green ED. Pendrin, the protein encoded by the Pendred syndrome gene (PDS), is an apical porter of iodide in the thyroid and is regulated by thyroglobulin in FRTL-5 cells. *Endocrinology* 2000; 141:839–845.
52. Challeton C, Branea F, Schlumberger M, Gaillard N, de Vathaire F, Badie C, Antonini P, Parmentier C. Characterization and radiosensitivity at high or low dose rate of four cell lines derived from human thyroid tumors. *Int J Radiat Oncol Biol Phys* 1997; 37:163–169.

53. Fabien N, Fusco A, Santoro M, Barbier Y, Dubois PM, Paulin C. Description of a human papillary thyroid carcinoma cell line. Morphologic study and expression of tumoral markers. *Cancer* 1994; 73:2206–2212.
54. Ito T, Seyama T, Hayashi Y, Hayashi T, Dohi K, Mizuno T, Iwamato K, Tsuyama N, Nakamura N, Akiyama M. Establishment of two thyroid carcinoma cell lines (8305C, 8505C) bearing p53 mutations. *Int J Oncol* 1994; 4:583–586.
55. Leibovitz A, Stinson JC, McCombs WB 3rd, McCoy CE, Mazur KC, Mabry ND. Classification of human colorectal adenocarcinoma cell lines. *Cancer Res* 1976; 36:4562–4569.
56. Fogh J, Wright WC, Loveless JD. Absence of HeLa cell contamination in 169 cell lines derived from human tumors. *J Natl Cancer Inst* 1977; 58:209–214.
57. Kruse CA, Mitchell DH, Kleinschmidt-DeMasters BK, Franklin WA, Morse HG, Spector EB, Lillehei KO. Characterization of a continuous human glioma cell line DBTRG-05MG: growth kinetics, karyotype, receptor expression, and tumor suppressor gene analyses. *In Vitro Cell Dev Biol* 1992; 28A:609–614.